Available online at www.sciencedirect.com

SCIENCE DIRECT®

Hydrometallurgy 75 (2004) 135–146

hydrometallurgy

www.elsevier.com/locate/hydromet

Aspects of gypsum precipitation in scaling waters

Shilpa Seewoo, Rob Van Hille, Alison Lewis*

Precipitation and Crystallisation Research Facility, Department of Chemical Engineering, University of Cape Town, South Africa

Received 26 April 2004; received in revised form 1 July 2004; accepted 20 July 2004

Abstract

The focus of this work is the control of the desupersaturation reactor in the Slurry Precipitation and Recycle Reverse Osmosis (SPARRO) process for desalinating water with a high calcium content. Three topics are covered in this paper: quantifying and controlling gypsum morphology, identifying and quantifying the crystallization phenomena in the reactor, and scaling up the reactor on the basis of a mixing time scale analysis. Experiments were carried out in batch mode, and the factors varied were seed morphology and quantity, stirrer speed and sulphate to calcium ratio. The measured responses were the crystal morphology, the time to reach equilibrium and the change in mean crystal size. Two distinct crystal morphologies (needles and platelets) were identified and appropriately quantified using an edge detection method. Both the quantity and the morphology of the seeds had a decisive influence on the seed morphology at equilibrium. The seed morphology at seed concentrations below 4% by volume also affected the time required to reach equilibrium. The proposed mechanism of desupersaturation is primarily a second order growth rate, with no nucleation taking place. There is evidence for the occurrence of attrition at higher Reynolds numbers. It is recommended that scale up take place to ensure that the relative influence of the characteristic mixing scales does not change.

Keywords: Mineral processing; Precipitation; Gypsum scale; Seeding; Crystal morphology; Scale up

1. Introduction

Partially treated gold mine waters, particularly from South Africa's gold mining operations, have high levels of calcium and sulphate ions. Lime, which is used for neutralisation of mine waters, is the source of calcium ions and the sulphate originates from oxidation of pyrite present in gold-bearing ores (Juby and Schutte, 2000). When the solubility of calcium sulphate dihydrate (commonly known as gypsum) is exceeded, precipitation of the salt is uncontrollable and scaling occurs. the Slurry Precipitation and Recycle Reverse Osmosis (SPARRO) process was developed in the early 1980s with the primary objective of desalinating water with a high calcium sulphate concentration efficiently and economically (Harries, 1985; Juby et al., 1992) (see Fig. 1). The process uses tubular cellulose acetate membranes in a seeded slurry system (Juby and Schutte, 2000) and has also been applied for the removal of heavy metals from aqueous

* Corresponding author. Fax: +27 216 504 091.
E-mail address: alison@chemeng.uct.ac.za (A. Lewis).

0304-386X/$ - see front matter © 2004 Elsevier B.V. All rights reserved.
doi:10.1016/j.hydromet.2004.07.003

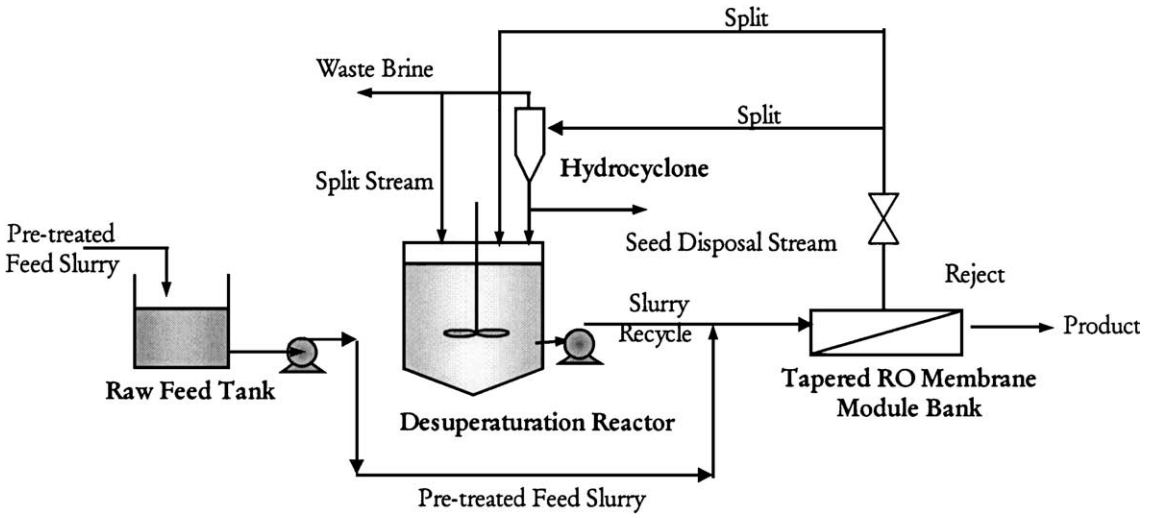

Fig. 1. Block flow diagram of the SPARRO process (Juby, 1994).

waste (Sluys et al., 2001) and to water softening (Verdoes and Hanemaaijer, 1994, 1996). Gypsum seeds are synthesized in a desupersaturation reactor and are supplied to the membranes together with the scaling water to be treated. The seeds provide preferential sites for gypsum precipitation; the permeate is a stream of scale-free water that is separated by reverse osmosis in the membrane and the reject stream is a supersaturated solution of gypsum, which is recycled to the reactor. The reactor should provide sufficient residence time for the supersaturated solution to reach equilibrium.

In previous research, Harries (1985) concluded that the tubular cellulose acetate (CA) membranes performed satisfactorily in the seeded slurry mode with no evidence of fouling, scaling or damage to the membranes. This was at seed slurry concentrations of approximately 40 g/L. However, later research (Juby and Schutte, 2000; Busby et al., 1991), reported problems with fouling, corrosion and hydrolysis. In addition, laboratory and pilot plant evidence has demonstrated premature membrane failure due to damage under a range of operating conditions. Thus, although the method is promising, many process and equipment-related questions remain unanswered. In particular, questions have been raised as to the effect of crystal morphology on the membrane damage. Thus, one of the main aspects of this research work was to investigate the issue of morphology control in gypsum scale and thus the focus of this work is the control of the desupersaturation reactor. Three topics are covered in this paper: quantifying and controlling morphology, identifying and quantifying the crystallization phenomena in the reactor, and scaling up the reactor on the basis of a mixing time scale analysis.

2. Literature review

2.1. Morphology control

From literature (Christoffersen et al., 1982) and experimental investigation (Lewis et al., 2002), it has been established that, depending on the experimental conditions, gypsum occurs as two primary morphologies: needles and platelets as shown in Fig. 2.

Lash and Burns (1984) produced both needle and platelet gypsum ($CaSO_4 \cdot 2H_2O$) crystals at room temperature by varying the initial reagent concentrations. The needle morphology was produced from solutions whose initial concentration was greater than 0.4 M in $CaSO_4$ while the platelet morphology was produced from solutions whose initial $CaSO_4$ concentration was less than 0.25 M. Conversely, Christoffersen et al. (1982), found that low concentrations (0.3 M $CaSO_4$) favoured the needle-like morphology, whereas high reagent concentrations (0.725 M $CaSO_4$) produced smoother surfaces. Liu and Nan-

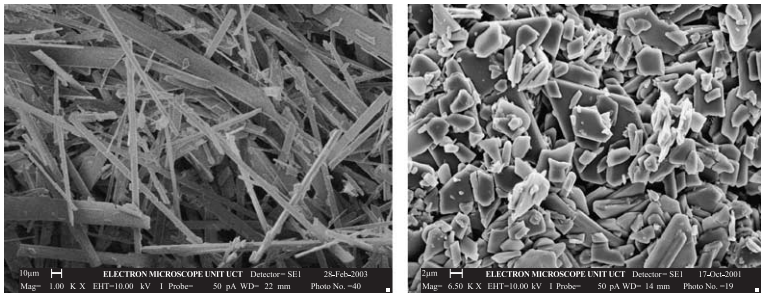

Fig. 2. Left: needle-like morphology, scale bar 10 μm. Right: plate type morphology, scale bar 2 μm.

collas (1970) added seed crystals to stable supersaturated solutions and formed needle-like monoclinic crystals 80–120 μm long in 0.1 M gypsum solutions and 30–50 μm long in 0.6 M solutions.

Lewis et al. (2002) focused on producing gypsum seed crystals of predictable size and morphology and investigated the effect of changing selected processing conditions on particle size distribution and crystal morphology. The needle-like morphology was generated under conditions of low supersaturation (supersaturation ratio 2.27) and was characterized by a lengthy induction time prior to nucleation. The average length of the crystals was in the region of 100 μm. The plate-like morphology was as a result of conditions of high supersaturation ratio, 10.86. This resulted in a significantly reduced induction time and a larger number of smaller (±25 μm) crystals. This morphology was characterized by a relatively larger specific surface area. The increase in induction time with decrease in supersaturation concurs with the results of Alimi et al. (2003).

2.2. Kinetics of seeded precipitation

Precipitation at low supersaturation levels is relatively slow and can be induced by seeding the solution. Kinetic relations for the growth of seed crystals from solution are well established and a power law-type formulation is most commonly used:

$$-\frac{dC_A}{dt} = kN_s(C_A - C^*)^n \quad (1)$$

where: k=reaction rate constant ($L^{n-1}/(\mathrm{mol}^{n-1}\mathrm{s})$), N_s=number of seed crystals, ($C_A - C^*$)=excess solute concentration (mol/L), n=order of growth.

The number of seed crystals affects the growth rate either through the total surface area in the case of a surface-reaction phenomenon or through surface-active sites in the case of screw dislocations.

Liu and Nancollas (1973) studied the seeded crystal growth of gypsum from supersaturated solution and found a reaction second order in relative supersaturation, σ. The effects of potential scale inhibitors including methyl enephosphoric acid and methylene phosphoric acid on the seeded growth of gypsum from supersaturated solutions were also studied (Liu and Nancollas, 1975). It was found that, in the presence of trace amounts of these additives, complete inhibition of growth for a certain period was achieved and thereafter the precipitation rate followed a second order law. They found that the duration of induction was significantly affected by the amount of seed crystals added.

Seeded precipitation of gypsum from supersaturated solutions both in pure water and in the presence of sodium chloride was studied by Brandse et al. (1977). They used 10% by volume of seed crystals and plotted the mean linear growth rate, R against the relative supersaturation. The relation between R and σ was given by a linear law for low values of σ; a parabolic law for higher values of σ and by orders higher than two for very high values of σ. They also found that the presence of sodium chloride in the precipitating system significantly increased the precipitation rate.

Seed preparation is an important step in seeded precipitation. Christoffersen et al. (1982) experimented with seeded gypsum precipitation using six batches of gypsum seed crystals. These seed crystals were prepared in different ways and had different specific surface areas and sizes. Their results showed

that the rate of growth varied for the different preparations of the gypsum seed crystals and that the overall rate of growth decreased with increasing mass of the crystals.

2.3. Mixing time scale analysis

The complex process of turbulent mixing can be broken down into simpler mixing steps, macro-, meso- and micro-mixing. Macro-mixing is defined as the process of mixing that takes place on the scale of the whole vessel. Macro-mixing defines residence time distributions and determines the environment concentrations for meso- and micro-mixing and conveys fluids that are undergoing meso-mixing and micro-mixing through environments where turbulence properties (such as the rate of energy dissipation, ε, and the scale of turbulence, Λ) vary. Meso-mixing represents the coarse-scale turbulent exchange between the fresh feed and its surroundings. The feed plume is coarse-scale relative to the micro-mixing scales and fine-scale compared to the scale of the system. Micro-mixing happens on the molecular scale and directly influences chemical reaction, nucleation and crystal growth, which are essentially molecular-level processes (Baldyga and Bourne, 1999). It has been experimentally found that, for a well-baffled tank and fully developed turbulence, the macro-mixing time, τ_M, is between three and five times the circulation time, τ_c.

$$\tau_m = 4\tau_c \tag{2}$$

where: τ_m=macro-mixing time (s), τ_c=circulation time (s).

For a vessel using an impeller with four pitched blades, the mixing rate determining circulation time, τ_c, which is the macro-mixing time, can be expressed as follows (Roelands et al., 2003):

$$\tau_c = \frac{V}{q_c} \tag{3}$$

where: V=vessel contents (m^3), q_c=pumping capacity of the impeller (m^3/s).

The pumping capacity of the impeller is given by (Roelands et al., 2003):

$$q_c = N_q N D^3 \tag{4}$$

where: N_q=flow number (taken as 0.73 for a pitched blade turbine, (Nienow, 1997)), N=impeller speed (rps), D=impeller diameter (m).

The meso-mixing time, which represents the time for the turbulent disintegration of the feed, is determined from (Torbacke and Rasmuson, 2001):

$$\tau_{meso} = a\left(\frac{\Lambda^2}{\varepsilon}\right)^{1/3} \tag{5}$$

where: a=constant (given as 2 (Baldyga et al., 1997)), Λ=macroscale turbulence (m), ε=local energy dissipation rate (m^2/s^3).

The macroscale turbulence is estimated (Torbacke and Rasmuson, 2001) by:

$$\Lambda = \sqrt{\frac{Q_b}{\pi u}} \tag{6}$$

where: Q_b=reactant flow rate (m^3/s), u=fluid velocity (m/s).

The local energy dissipation rate is given by (Torbacke and Rasmuson, 2001):

$$\varepsilon = a\frac{N_p N^3 D^5}{V} \tag{7}$$

where: a=constant (given as 2 (Baldyga et al., 1997), N_p=power number (taken as 1.5 for a pitched blade (Uhl and Gray, 1966)), N=impeller speed (rps), D=impeller diameter (m).and:

$$N_p = \frac{Pg}{\rho N^3 D^5} \tag{8}$$

where: P=power (W), g=acceleration due to gravity (9.81 ms^{-2}), ρ=liquid density (kg/m^3).

The micro-mixing time is determined from (Baldyga and Bourne, 1989):

$$\tau_{micro} = 17.24\sqrt{\frac{\gamma}{\varepsilon}} \tag{9}$$

where: γ=kinematic viscosity (m^2/s), ε=local energy dissipation rate (m^2/s^3).

3. Materials and methods

The 5 L lab-scale desupersaturation reactor was designed based on the literature review with the

Table 1
Tank geometry and impeller specifications

Number of baffles	four, 90° to each other
Tank diameter, T (m)	0.22
Baffle width	0.1 T
Draft tube diameter	0.5 T
Draft tube height	0.5 T
Tank bottom geometry	rounded bottom
Height of liquid (H)	0.773 T
Material of construction of tank	Perspex
Impeller type	axial, four-pitched-blades
Pitch	45°
Impeller diameter (D)	0.33 T
Blade width	0.2 D
Impeller clearance	0.33 H
Material of construction of impeller	stainless steel

aim of achieving good solid–liquid suspension. Table 1 gives the specifications of the tank and impeller.

3.1. Experimental design

Experiments were carried out using a half-replicate 2^4 factorial design and axial point experiments, respectively. Seed morphology, quantity, pH, stirrer speed and sulphate to calcium ratio were varied. The experimental details are given in Table 2. Some levels were not feasible due to negative values or because of physical constraints. In these cases, the +1 or −1 levels were used. In this work, the model fitting for the full statistical design is not reported, so only the relevant experiments reported here are detailed in Table 3.

3.2. Experimental procedure

All experiments A to D were carried out in batch mode to investigate the effects of the factors

Table 2
Levels of factors varied in experiments

Factor/level	−2	−1	0	1	+2
Seed quantity [% by volume] (SQ)	N/A	1	4	7	10
pH	1	4	7	10	N/A
Impeller speed [rpm] (N)	N/A	300	500	700	900
Sulphate to calcium molar ratio (SCR)	N/A	1	4	7	10

Table 3
Experiments using both needle- and plate-like seed crystals

Experiment for needle	Experiment for plate	SQ	pH	N	SCR
A1	B1	1	1	1	1
	B3	0	0	0	0
	B5	0	0	0	0
A11	B11	−1	−1	−1	−1
	C5	0	0	−1	0
	C6	0	0	+2	0
	D1	−1	0	0	−1
	D2	0	0	0	−1
	D3	+1	0	0	−1

independently. The initial concentration of calcium ions was 0.03 M, a concentration that would typically occur in mine water. The reactor was initially filled with 2.5 L of 0.06 M calcium chloride solution (prepared by dissolving high-purity anhydrous calcium chloride (Merck) in distilled water).

Needle-like or plate-like crystals were synthesized using experimental conditions that had been established in prior scoping studies (Lewis et al., 2002). The particle size distribution of the seed crystals was determined using a laser diffraction technique (Malvern Mastersizer, model MAM 5002). A small sample of the seeds was filtered through a Millipore 0.45 μm filter using a vacuum pump. These crystals were dried for scanning electron microscopy. Preset quantities of seed crystals were transferred into the reactor. The pH of the system was controlled by a custom-made pH controller. The position of the probe was outside the draft tube, in the annular region of the vessel, far from the acid and base inlet. NaOH (0.05 M) and HCl (0.05 M) solutions were used to adjust the pH of the system. These solutions were prepared using analytical grade chemicals (Merck) and distilled water. The base and acid feed inlet in the reactor were located close to the impeller to ensure rapid dispersion.

The experiment was initiated by pumping (Masterflex peristaltic pump, model 7521-47) 2.5 L of sodium sulphate solution into the reactor at 9.5 mL/s. The feed point of sodium sulphate was kept close to the impeller to ensure good dispersion. The pH controller was activated and readings from a conductivity meter (Radiometer analytical, Ion

check 30) were taken at 1-min intervals. The conductivity probe was inserted in the reactor lid at a position far from the sodium sulphate feed point.

When the readings from the conductivity meter stabilised, samples were withdrawn from the sample port using a syringe. For all the experiments, the samples were taken from the same position in the reactor. The particle size distribution of the sample was measured using a mastersizer (Malvern Mastersizer, model MAM 5002). Samples of crystals were filtered through a Millipore 0.45μm filter using a vacuum pump and left to dry for 96 h for scanning electron microscopy.

3.3. Seed preparation: needle-like seed crystals

Needle-like seed crystals were prepared by pumping (Masterflex peristaltic pump, model 7521-47) 0.08 M sodium sulphate solution at 9.5 mL/s into a 0.08 M calcium chloride solution. Analytical grade chemicals (Merck) and distilled water were used to prepare these reagents, which resulted in a weakly supersaturated solution (0.04 M, supersaturation ratio of 2.27) of calcium and sulphate ions. Therefore, a long induction time and large volumes of reagents were required to produce a small quantity of seed crystals. A 15 L tank was used as the reacting vessel and a four-pitched blade impeller, identical to that used in the desupersaturation reactor, was used to agitate the reagents at 500 rpm. Each batch of the 15 L preparation was left for 24 h and yielded 200 mL of crystals (4% by volume in the 5 L desupersaturation reactor). These crystals were filtered for use in the batch desupersaturation experiments.

3.4. Seed preparation: plate-like seed crystals

Plate-like seed crystals were prepared by direct addition of 0.4 M sodium sulphate solution to 0.4 M calcium chloride solution. These reagents resulted in a highly supersaturated solution (0.2 M, supersaturation ratio of 10.86) of calcium and sulphate ions. Therefore, a short induction time and small volumes of reagents were used to produce a large quantity of seed crystals. A 250 mL beaker was used as the reacting vessel and a magnetic stirrer at 500 rpm was used for mixing the reactants. Each batch of the 250 mL preparation was agitated for 1 min and yielded 25 mL of crystals (0.5% by volume in the 5 L desupersaturation reactor). These crystals were filtered and used in the desupersaturation reactor. Dry samples of the seed crystals were ground and analysed by powder X-ray Diffraction (Philips, model PW1050).

3.5. Responses and methods of analysis

The three responses that were measured were the crystal morphology, the time to reach equilibrium and the percentage crystal growth.

3.6. Quantification of morphology

For this work, it was important to be able to distinguish between the two different crystal morphologies, as well as to quantify the morphology in

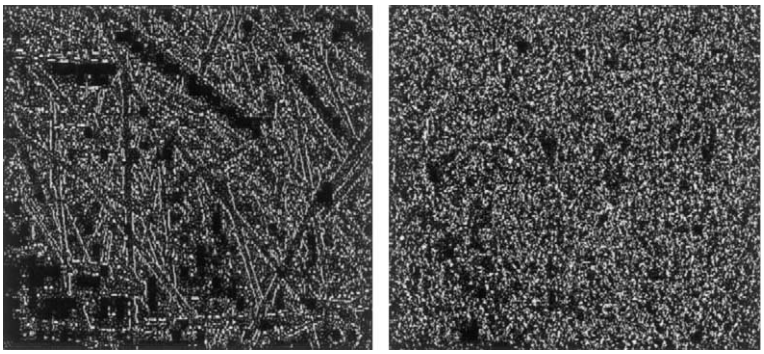

Fig. 3. Processed images. Left: needle-like seed crystals. Right: plate-like seed crystals.

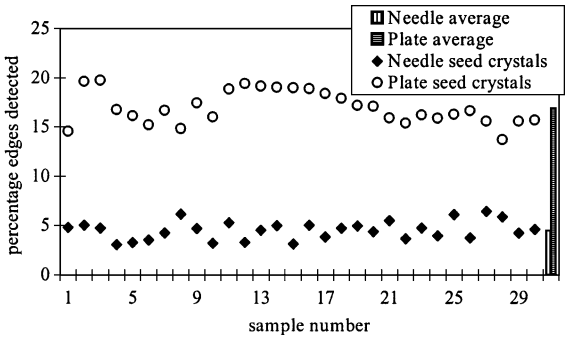

Fig. 4. Percentage of edges detected for needle- and plate-like seed crystals showing data points and averages.

some way, especially since using a laser diffraction method with the needle morphology is not considered to be very reliable. This was achieved using a digitised SEM image. Dry samples of the crystals were mounted on stubs with carbon glue and coated with gold palladium alloy. The SEM images were taken at a magnification of 1000× and digitised using Matlab 6.5 with Image Processing Toolbox. The algorithm-generated digital images of the edges detected and calculated the percentage of edges detected over the digital image. Thirty samples of each morphology were used. Ten different pictures of each sample were analysed and an average taken.

3.7. Time to reach equilibrium

A conductivity meter was used to provide an accurate, online measurement of the conductivity of the solution, thus obviating the need to withdraw samples from the reactor. The system was considered to have reached equilibrium when the conductivity meter readings were fully stabilised.

3.8. Percentage crystal growth

The mass weighted mean size of the initial seed crystals, $d(4,3)_{\text{seeds}}$, and the mass weighted mean size of crystals withdrawn from the equilibrium solution, $d(4,3)_{\text{equil}}$, were used to calculate the percentage crystal growth:

$$\text{percentage crystal growth} = \frac{(d[4,3])_{\text{equil}} - (d[4,3])_{\text{seeds}}}{(d[4,3])_{\text{seeds}}} 100 \quad (10)$$

An average of three readings taken from the Malvern Mastersizer for each crystal sample was used for the mean particle size. Crystal samples were placed in an ultrasonic bath (EIA, model CP823) for 3–5 min at 25 °C at 90% power prior to size measurement to prevent particle agglomeration. Propanol was used as the medium due to its favourable dispersant properties.

4. Results and discussion

4.1. Seed crystal purity

Representative samples of both morphologies were analysed by X-ray diffraction to determine the composition and purity of the material. The results confirmed that the composition of both sets of samples was the same and both were identical to that of analytical grade gypsum.

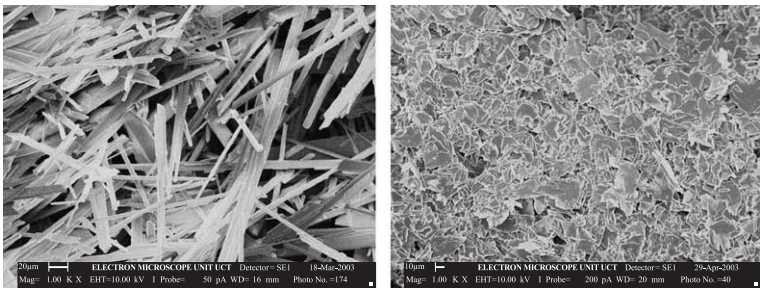

Fig. 5. Left: crystals from experiment A1, Right: experiment B1. Scale bar 20 μm.

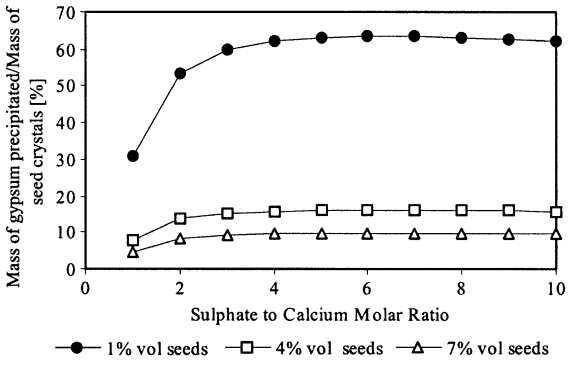

Fig. 6. Effect of seed quantity on mass precipitated per mass of seeds.

4.2. Quantification of gypsum morphology

The processed images corresponding to Fig. 2 are shown in Fig. 3. The number of edges detected for the plate-like morphology is 17.0±1.7 compared to 4.5±0.94 for the needle morphology. The results (Fig. 4) show that there was no overlap between the percentage edges detected for needle-like and plate-like crystals, confirming that two distinct morphologies have been identified and appropriately quantified.

4.3. Controlling morphology

The morphology of the seed crystals was shown to have a decisive influence on the seed morphology at equilibrium. Fig. 5 shows the morphology of gypsum crystals harvested from the reactor at equilibrium for experiments A1 and B1, respectively, for which the operating conditions were identical and only the seed morphology differed. Image analysis of the needle morphology in Fig. 5 yielded a low percentage edges detected of 4.75±1.02, while analysis of the plate morphology in Fig. 5 generated a higher percentage edges detected of 15.16±2.06. This quantitative analysis also demonstrates that the final crystal morphology under these conditions is determined by the morphology of the seed crystals used in the process.

As expected, the morphology at equilibrium was also influenced by the seed quantity. As the seed concentration increased, the total available surface area for precipitation increased, resulting in a smaller mass of precipitation on each seed and a smaller potential for a change in morphology. Fig. 6 shows the relationship between the amount of gypsum precipitated from solution per mass of seeds and the initial volume percentage of seeds for a range of sulphate to calcium molar ratios.

Based on the results presented above, the choice of an appropriate seed crystal morphology and quantity has implications for the kinetics of gypsum precipitation and the final morphology of the crystals. These aspects were not explicitly examined in previous work on the SPARRO process (Juby, 1994). In fact, in previous work on the SPARRO process, 1.76% by volume of seeds were added to the reactor (Juby, 1994). Under these conditions, control of morphology would be reduced and reaction kinetics would be slow. Current work is investigating morphology control under continuous operating conditions.

4.4. Identification of crystallization phenomena in the reactor

4.4.1. Effect of seed morphology on kinetics

The morphology of the seed crystals had a significant effect on the kinetics of desupersaturation

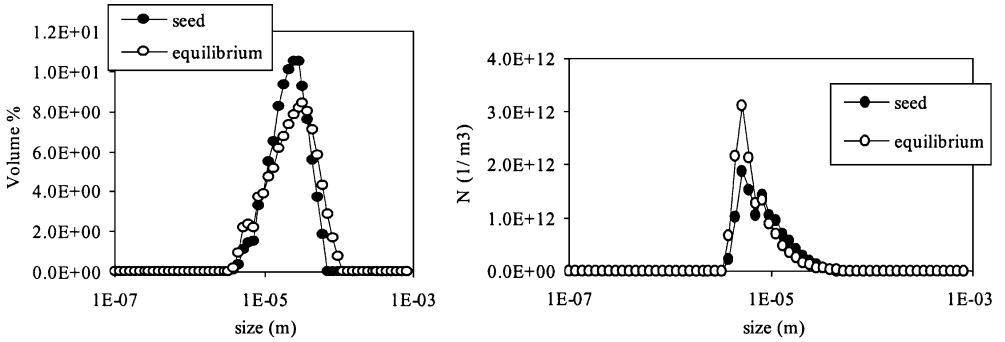

Fig. 7. PSD of plate-like seeds and crystals present at equilibrium from experiment B5. Left: volume distribution. Right: number distribution.

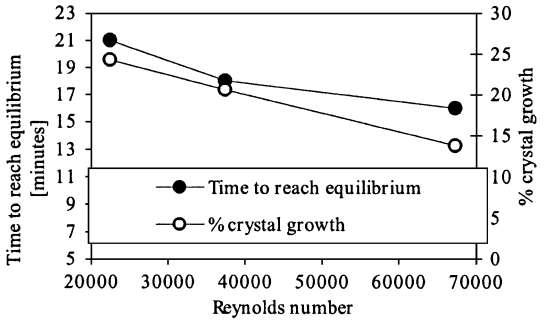

Fig. 8. Reynolds number (defined in Eq. (12)) versus time to reach equilibrium and percentage of crystal growth.

at low seed concentrations, where the time required to reach equilibrium in experiments seeded with needle-type crystals was up to three times longer than for the corresponding experiment using plates. This can be attributed to the higher specific surface area of the plates. At seed concentrations above 4% by volume, this effect was not significant, suggesting that the total surface area available was high enough not to be rate-limiting.

4.4.2. Evidence for growth

The particle size distribution for gypsum seed crystals and those present in the reactor at equilibrium for the B5 experimental run is shown in Fig. 7. The mass weighted mean size ($d(4,3)$) of the seed crystals was 24.43 μm. At equilibrium, the $d(4,3)$ had increased to 28.94 μm. The increase in mean particle size is evidenced by a rightwards shift in the peak of the graph. This trend was consistent through all the experimental runs and suggests that the mechanism of desupersaturation is precipitation onto existing seed material, resulting in an increase in particle size.

4.4.3. Evidence for attrition

Calculation of the zeroth moment of the particle size distribution data from

$$m_0 = \int_{0^-}^{\infty} l\, n(l) dl \tag{11}$$

where, m_0=zeroth moment (#/m^3), l=particle size (m), $n(l)$=number density (#/m^{-4}) indicates that there is a 20% increase in the total number of particles over the course of the experiment (from m_0=1.15E+13/m^3 at the start to m_0=1.38E+13/m^3 at equilibrium). The only two mechanisms that could be responsible for this increase are nucleation (the birth of new particles) and attrition (breakage of existing particles into smaller ones). For the conditions in which the experiments were carried out, it is unlikely that nucleation is the source of the increase in particle number. The highest supersaturation ratio was still relatively low (S=2.6) and under these conditions, the primary nucleation rate would be significantly lower than the growth rate (Sohnel and Garside, 1992). Previous work has also found that nucleation processes in seeded precipitation of gypsum were unimportant (Christoffersen et al., 1982), who investigated gypsum precipitation from solutions at supersaturation ratios between

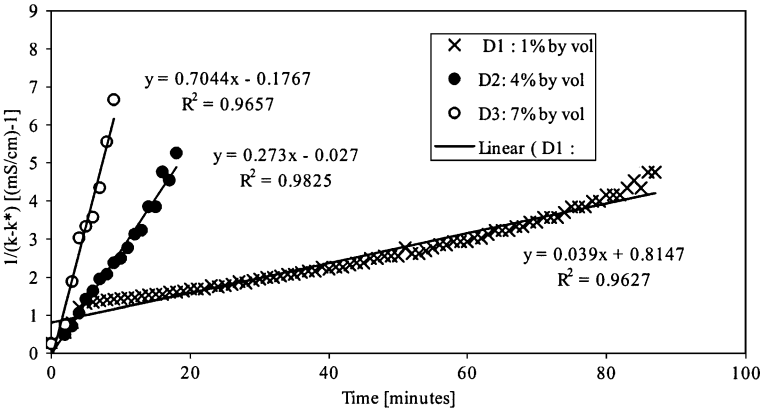

Fig. 9. Determination of rate constants for experiments D1–D3.

Table 4
Rate constants obtained from experiments D1–D3

Experiment	Seed quantity (volume %)	Seed quantity (#)	Rate constant, P' [cm(mS min)$^{-1}$]
D1	1	2.31*E*+09	0.039
D2	4	9.23*E*+09	0.273
D3	7	1.62*E*+10	0.704

1.03 and 2. Mullin (2001) found that below a critical supersaturation ratio of 4, the nucleation rate is exceptionally slow.

In support of the particle attrition hypothesis is the increase in the total number of particles, as well as the effect of increasing Reynolds number on time to reach equilibrium and thus on the reaction rate. The Reynolds number was increased by increasing the rotational speed of the impeller and is defined here as:

$$Re = \frac{D^2 N \rho}{\mu} \tag{12}$$

where, Re=Reynolds number, D=impeller diameter (m), N=impeller rotational speed (rps), ρ=liquid density (kg/m^3), μ=viscosity (kg/ms).

If attrition is an important mechanism, increasing the Reynolds number would have increased the number of particles, thereby increasing the available surface area and thus reducing the time to reach equilibrium. This is illustrated in Fig. 8 for experiments C5, B3 and C6. This effect would also have reduced the growth rate at higher Reynolds numbers, as evidenced in Fig. 8.

4.4.4. Effect of seed quantity on reaction rate

The seed quantity determined the available surface area upon which precipitation could occur and thus played a significant role in the rate of desupersaturation. In experiments D1–D3, which were conducted using plate-like seed crystals at 1%, 4% and 7% by volume and a sulphate to calcium ratio of 1:1, equilibrium was reached in 152, 65 and 48 min, respectively. In order to quantify the effect of seed quantity on reaction rate, the equation of Brandse et al. (1977) was modified to include conductivity, rather than solute concentration terms. The modified form is represented below:

$$-\frac{d\kappa}{dt} = P' (\kappa - \kappa^*)^n \tag{13}$$

where: κ=conductivity of the solution at time t (mS cm^{-1}), κ^*=conductivity of the solution at equilibrium conditions (mS cm^{-1}), P'=kinetic rate constant [cm(mS min)$^{-1}$ if n=2], n=order of the growth.

The rate constant was determined by integrating and linearising the equation and determining the slope of the plot of $(1/(\kappa-\kappa^*))$ versus t. The resulting plots are shown in Fig. 9 and the rate constants are shown in Table 4.

The plots are linear for n=2, confirming that the growth is second order. This result corresponds with those of Liu and Nancollas (1970, 1973, 1975), Brandse et al. (1977), Christoffersen et al. (1982) and Çetin et al. (2001).

4.5. Mixing time analysis and scale up

Macro-, meso- and micro-mixing times were calculated for experiments C5, B3 and C6 and related to the desupersaturation time percentage growth for each experiment. The values are given in Table 5.

Since the reaction time (or desupersaturation time) is greater than all of the characteristic mixing times in every case, this suggests that the reactor is well mixed and that the precipitation reaction takes place throughout the reactor (Sohnel and Garside, 1992). Although the elementary processes (reaction, nucleation and growth) comprising the overall precipitation process are molecular level processes, and thus are influenced directly only by the micro-mixing (Baldyga and

Table 5
Mixing times for experiments C5, B3 and C6

Experiment	Macro-mixing time (s)	Meso-mixing time (s)	Micro-mixing time (s)	Desupersaturation time (min)	Growth (%)
C5	6.9	0.09	0.06	21	24.25
B3	4.1	0.05	0.03	18	20.61
C6	2.3	0.02	0.01	16	13.79

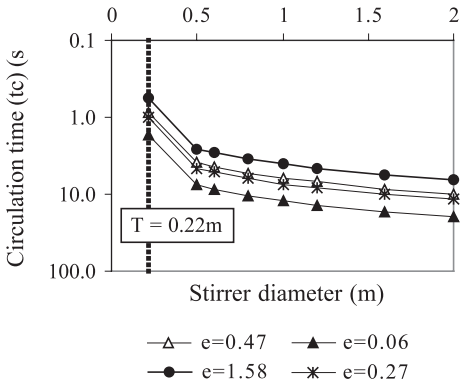

Fig. 10. Effect of scale up at constant local energy dissipation rate on circulation time and tip speed.

Orciuch, 2001), in this case, the reaction time is sufficiently slow that micro-mixing is not rate-limiting. In addition, owing to the relatively soluble nature of gypsum (solubility product (K_{sp})=2.4×10^{-5}) and the presence of seeds in the system, nucleation is not significant in this process, and the growth kinetics are dominant. Thus, the time scale of interest in the process is the macro-mixing time. Accordingly, when scale up is carried out, it is important to ensure that the macro-mixing time does not increase to such an extent that it becomes larger than the reaction time. In other words; the relative magnitude of the characteristic mixing times and the chemical reaction time should not change with scale up.

For example, in previous work on the same reactor, Seewoo (2003) found that suitable operating conditions were those of experiment B3, (T=0.22 m, N=8.3 s^{-1} and a local energy dissipation rate of ε=0.27 m^2/s^3). If the reactor is scaled up to, for example, T=1 m and the same local energy dissipation rate is maintained, the macro-mixing time will increase only to 7.5 s and the reactor can thus still be considered to be well mixed in relation to the reaction time. The change in macro-mixing time with change in scale is illustrated in Fig. 10 for a range of reactors from 0.22 m diameter (lab scale) to 2 m diameter. Further work on the topic of scale up for this process is ongoing.

In this work, the optimum crystal size and morphology was produced under the conditions of experiment B3, at a stirrer speed of 500 rpm (Re=3.7×10^4) a tip speed of N=8.3 s^{-1} and a local energy dissipation rate of ε=0.27 m^2/s^3 (Seewoo, 2003). In order to maintain this local energy dissipation rate at a larger scale, the tip speed and thus circulation time will need to be reduced, Further work on the topic of scale up for this process is ongoing.

Nomenclature

a	constant for meso-mixing and local energy dissipation (=2 (Baldyga et al., 1997))
C^*	equilibrium solute concentration (mol/L)
C_A	solute concentration (mol/L)
D	impeller diameter (m),
$d_{4,3}$	mass weighted mean size (m)
g	acceleration due to gravity (9.81 ms^{-2})
H	height of liquid (m)
k	reaction rate constant (L^{n-1}/(mol^{n-1}s))
K_{sp}	solubility product
l	particle size (m)
m_0	zeroth moment (#)
$n(l)$	number density (m^{-4})
n	order of growth
N	impeller speed (rps)
N_p	power number (taken as 1.5 for a pitched blade (Uhl and Gray, 1966))
N_q	flow number (taken as 0.73 for a pitched blade turbine, (Nienow, 1997))
N_s	number of seed crystals (#)
P	power (W)
P'	kinetic rate constant [cm(mS min)$^{-1}$ if n=2]
Q_b	reactant flow rate (m^3/s)
q_c	pumping capacity of the impeller (m^3/s)
R	linear growth rate (m/s)
Re	Reynolds number
S	supersaturation ratio (C_A/C^*)
T	tank diameter (m)
u	fluid velocity (m/s)
V	vessel contents (m^3)
κ	conductivity of the solution at time t (mS cm^{-1})
κ^*	conductivity of the solution at equilibrium conditions (mS cm^{-1})
γ	kinematic viscosity (m^2/s)
ε	local energy dissipation rate (m^2/s^3)
ρ	liquid density (kg/m^3)
μ	viscosity (kg/ms)
σ	relative supersaturation
τ_c	circulation time (s)
τ_m	macro-mixing time (s)
Λ	macroscale turbulence (m)
τ_{meso}	meso-mixing time (s)
τ_{micro}	micro-mixing time (s)

References

Alimi, F., Elfil, H., Gadri, A., 2003. Kinetics of the precipitation of calcium sulfate dihydrate in a desalination unit. Desalination 157, 9–16.

Baldyga, J., Bourne, J.R., 1989. Simplification of micromixing: I. Derivation and application of new model. The Chemical Engineering Journal 42, 83–92.

Baldyga, J., Bourne, J.R., 1999. Turbulent Mixing and Chemical Reactions. John Wiley and Sons, West Sussex.

Baldyga, J., Orciuch, W., 2001. Some hydrodynamic aspects of precipitation. Powder Technology 121, 9–19.

Baldyga, J., Bourne, J.R., Hearn, S.J., 1997. Interaction between chemical reactions and mixing on various scales. Chemical Engineering Science 52, 457–466.

Brandse, W.P., Van Rosmalen, G.M., Brouwer, G., 1977. The influence of sodium chloride on the crystallisation rate of gypsum. Journal of Inorganic and Nuclear Chemistry 39, 2007–2010.

Busby, R.W., Juby, G.J.G., Pulles, W., Nel, S., 1991. The evaluation of slurry reverse osmosis for the desalination of calcium sulphate scaling mine service water. Report to the Water Research Commission by the Chamber of Mines Research Organisation.

Çetin, E., Eroglu, I., Ozkar, S., 2001. Kinetics of gypsum formation and growth during the dissolution of colemanite in sulfuric acid. Journal of Crystal Growth 231, 559–567.

Christoffersen, M.R., Christoffersen, J., Rosmalen, G.M., Weijnen, M.P.C., 1982. Crystal growth of calcium sulphate dihydrate at low supersaturation. Journal of Crystal Growth 58, 585–595.

Harries, R.C., 1985. A field trial of seeded reverse osmosis for the desalination of a scaling-type mine water. Desalination 56, 227–236.

Juby, G.J.G., 1994, Development of a novel membrane desalination technique for treating calcium sulphate scaling mine water: the SPARRO process, PhD thesis, University of Pretoria, South Africa.

Juby, G.J.G, Schutte, C.F., 2000. Membrane life in a seeded slurry reverse osmosis system. Water SA, vol. 26, (No. 2), April 2000, 239–248.

Juby, G.J.G., Pulles, W., Busby, R.W., 1992. Development of the Slurry Precipitation and Recycle Reverse Osmosis (SPARRO) Technology For Desalinating Scaling Mine Waters. Water Science and Technology 25 (10), 177–192.

Lash, J.E., Burns, G., 1984. Heats of crystallization of $CaSO_4 \cdot 2H_2O$. Bulletin des Societes Chimiques Belges 93, 271–279.

Lewis, A., Nathoo, J., Seewoo, S., Lacour, S., 1970. Prevention of Scaling in Mine Waters Using Slurry Precipitation and Recycle Reverse Osmosis (SPARRO). 15th International Symposium on Industrial Crystallisation, Sorrento, Italy, 15–18th September.

Liu, S., Nancollas, G.H., 1970. The kinetics of crystal growth of calcium sulfate dihydrate. Journal of Crystal Growth 6, 281–289.

Liu, S., Nancollas, G.H., 1973. Linear crystallization and induction-period studies of the growth of calcium sulphate dihydrate crystals. Talanta 20, 211–216.

Liu, S., Nancollas, G.H., 1975. A kinetic and morphological study of the seeded growth of calcium sulfate dihydrate in the presence of additives. Journal of Colloid and Interface Science 52, 593–601.

Mullin, J.W., 2001. Crystallization. Butterworth-Heinemann, Boston.

Nienow, A.W., 1997. On impeller circulation and mixing effectiveness in the turbulent flow regime. Chemical Engineering Science 52, 2557–2565 (15 August).

Roelands, C.P.M., Derksen, J.H., Kramer, H.J.M., Jansens, P.J., 2003. Analysis of mixing in a typical experimental set-up to measure nucleation rates of precipitation processes. Chemical Engineering and Technology 26, 296–303.

Seewoo, S., 2003. Morphology control in gypsum precipitation, MSc Thesis, University of Cape Town.

Sluys, J.T.M., Bakkenes, H.W., van Marwijk, W.G., van Tongeren, W.G.J.M., Hanemaaijer, J.H., 2001. MAAS masters metals, TNO, P.O. Box 6050, NL-2600 JA Delft.

Sohnel, O., Garside, J., 1992. Precipitation: Basic Principles and Industrial Application. Butterworth-Heinemann, Oxford.

Torbacke, M., Rasmuson, A.C., 2001. Influence of different scales of mixing in reaction crystallisation. Chemical Engineering Science 56, 2459–2473.

Uhl, V.W., Gray, J.B., 1966. Mixing. Academic Press, New York.

Verdoes D., Hanemaaijer, J.H., 1994. Method and appliance for removing at least one constituent from solution, European Patent EP 0669898.

Verdoes, D., Hanemaaijer, J.H., 1996. Membrane-assisted Crystallization: A New Hybrid Process Exemplified by the Softening of Water. In: Ulrich, J., Wangnick, K. (Eds.), Bremen International Workshop on Industrial Crystallization, pp. 92–99.